LAWRENCE
LIVERMORE
NATIONAL
LABORATORY

LLNL-JRNL-712618

Attainment of a stable, fully detached plasma state in innovative divertor configurations

M. V. Umansky, B. LaBombard, D. Brunner, M. E. Rensink, T. D. Rognlien, J. L. Terry, D. G. Whyte

November 30, 2016

Physics of Plasmas

Disclaimer

Attainment of a stable, fully detached plasma state in innovative divertor configurations

M. V. Umansky,[1] B. LaBombard,[2] D. Brunner,[2] M.E. Rensink,[1] T.D. Rognlien,[1] J.L. Terry,[2] and D.G. Whyte[2]

[1)] *Lawrence Livermore National Laboratory, Livermore, CA 94550*

[2)] *MIT Plasma Science and Fusion Center, Cambridge, MA 02139*

(Dated: 28 November 2016)

A computational study of long-legged tokamak divertor configurations is performed with the edge transport code UEDGE. Several divertor configurations are considered, with radially or vertically extended, tightly baffled, outer divertor legs, and with or without a secondary X-point in the divertor leg volume. For otherwise identical conditions, a scan of the input power from the core plasma is performed. As the power is reduced to a threshold value, the plasma in the outer leg transitions to a fully detached state, which defines the upper limit on the power for detached divertor operation. Reducing the power further results in the detachment front shifting upstream but remaining stable. At low power the detachment front eventually moves all the way to the primary X-point, which is usually associated with degradation of the core plasma, and this defines the lower limit on the power for the detached divertor operation. For the studied parameters, for long-legged divertors, the detached operation window is quite large, in particular for the X-point target configuration using a secondary X-point in the divertor leg volume, allowing a factor of 5-10 variation in the input power. For the same parameters, for the standard divertor configuration, the detached operation window is very small, or even non-existent. The present modeling results suggest the possibility of stable fully detached divertor operation for a tokamak with tightly baffled extended divertor legs.

I. INTRODUCTION

Realization of fusion as an energy source hinges on successful solution of numerous engineering and technological challenges. For a tokamak-based fusion reactor, managing the heat flux arriving at the divertor plates is one critical issue that will need to be addressed.

Modern tokamaks operate with the magnetic divertor, which strongly improves the performance compared with the limiter tokamak operation used in the early days. The standard tokamak divertor is formed by a toroidal divertor coil current, which, combined with the toroidal plasma current, leads to formation of magnetic flux surfaces with an X-point (the null-point of poloidal magnetic field), and a magnetic separatrix between the core plasma region and the scrape-off layer (SOL) and private-flux (PF) regions. The heat and particle flux exhausted from the core plasma flows poloidally in the scrape-off layer toward the divertor chamber, and a large fraction of this flux is intercepted by divertor target plates. Thus in the divertor configuration plasma-material interactions are largely removed from the main plasma, which is advantageous for the main plasma. However, there is a problem with this picture: the width of the scrape-off layer is small and consequently the divertor heat flux, per unit area, is large.

Projections to future machines indicate unacceptably large power fluxes on the divertor material surfaces. The SOL power width λ_{sol} is on the order of a few mm in present-day tokamaks, and based on the present experiments, λ_{sol} scales as $1/B_{pol}$; but there is no scaling with the tokamak size[1]. On the other hand, the exhaust power of a tokamak does scale with the size, generally increasing with the plasma volume, so the overall trend for the divertor heat flux looks quite unfavorable for larger machines. Thus for next-generation tokamak some new solutions will be needed for the divertor.

For a given tokamak design, several key parameters are already fixed, e.g., the exhaust power, major radius, minor radius; and, based on the presently known scaling[1], λ_{sol} is also fixed. The degrees of freedom available for optimizing the divertor include the divertor leg length, the divertor plate tilt and shaping, and the divertor poloidal flux expansion.

From the geometric considerations, one can try to increase the plasma-wetted area A_w on the target plate, which should reduce the heat flux on the plate, by increasing the plate tilt angle and/or by increasing the poloidal magnetic flux expansion. However, for either method, with increasing A_w the grazing angle γ between the total magnetic field and the surface becomes small. Due to the surface roughness, using a too small angle γ would lead to non-uniform heating of the surface. For realistic quality of the surface, the minimum grazing angle has been estimated to be on the order of

1°. Reducing the grazing angle γ to the smallest possible value γ_0 sets the limit for increasing A_w for a given major radius of the target plate R_t; for further increasing of A_w the major radius of the target plate R_t would need to be increased[2]. Thus an advantage of radially extended divertor legs is making possible larger plasma-wetted area A_w; however for a practical tokamak divertor design this geometric advantage alone would surely be insufficient if the characteristic P/R ratio needs to be reduced by an order of magnitude to yield acceptable levels of heat flux on the divertor plate.

Beyond increasing A_w by plate tilting and poloidal flux expansion, extra divertor coils can modify the divertor poloidal magnetic field topology, and some innovative divertor ideas proposed along these lines in recent years suggest using auxiliary X-points[3,4] or higher-order null-points[5,6]. A recent idea is the X-point target divertor (XPTD) configuration[7] which combines the radially extended divertor leg with a secondary X-point in the divertor volume.

These innovative divertor configurations might offer some geometric advantage in the poloidal flux expansion, connection length, and plasma-wetted area A_w[2,5,6]. However, what is perhaps even more interesting, the plasma physics itself can be affected in innovative divertor configurations in ways favorable for mitigating the divertor heat flux, e.g., through effects of ion orbit loss[8] and MHD instabilities[9].

Beyond plasma physics, atomic physics can also be a very significant player in the divertor, in particular because of its effects on divertor plasma detachment. In the detached state, plasma is not in contact with the divertor target plates, as it is cushioned by a layer of neutral gas, and the impinging energy flux is dissipated by radiation. Although viewed as a desirable mode of divertor operation in the early days of divertor research, the fully detached divertor has been found in tokamak experiments (and similarly in modeling) to be usually a very fragile mode of operation, easily leading to a MARFE[10]. MARFEs negatively affect the main plasma performance, usually resulting in loss of energy confinement or plasma disruption. For this reason, ITER, for example, is envisioned to operate only in partial but not in full divertor detachment mode, in spite of severe divertor heat flux problems anticipated for ITER[11].

The effects of innovative divertor configurations on plasma detachment have so far been largely unexplored, although some studies have started to emerge very recently[12]. The results of the investigation presented in this report are based on an axisymmetric 2D fluid model of tokamak edge plasma implemented in the UEDGE code that uses an ad-hoc representation of the anomalous radial transport[13]. On the other hand, the model includes a rather accurate representation of the

magnetic geometry, parallel transport, and atomic physics, which together allows capturing the key effects of the divertor configuration on the divertor plasma detachment. In the comparative study described here, UEDGE is applied to several different divertor configurations for otherwise similar parameters, based on the design of the ADX tokamak concept[7]. As described below, the results obtained in this study point to the beneficial role of radially - or even vertically - extended, tightly baffled, divertor leg geometry, and a secondary X-point in the divertor leg, for entering and maintaining a stable fully detached divertor regime.

II. SIMULATION SETUP

Four divertor cases are considered here, all based on the geometry and parameters of the ADX tokamak design[7]. Starting from very similar ADX MHD equilibria, target plates are introduced at various locations to produce (i) a X-point target divertor (XPTD), (ii) a super-X divertor (SXD), (iii) a long vertical leg divertor (LVLD), and (iv) a standard vertical plate divertor (SVPD); see Fig. (1). The SOL radial temperature and density profiles are set to match the ADX projections, which are based on the existing scalings. A radially growing profile for the density diffusion coefficient $D_\perp$ is used to match the expected mid-plane radial plasma density $n_{e,i}$ profile width 5 mm; and a spatially constant $\chi_{\perp,e,i}$ is used to achieve a 3 mm width of the mid-plane $T_{e,i}$ profiles. The plasma density at the core interface is fixed at 1×10^{20} m^{-3}, and the resulting value at the separatrix is close to 0.5×10^{20} m^{-3}; see Fig. (2). This is at the low end of separatrix densities anticipated for ADX, representing the most challenging upstream conditions for divertor power handling. Unless stated otherwise, the runs use fully recycling wall boundary conditions and perfect neutral particle albedo on all material surfaces, which is appropriate to simulate steady state reactor conditions. A fluid neutral model is employed. In all code runs a 1% carbon seed impurity is used, in the "fixed fraction" model[14]. Note that this impurity level, if fully ionized, would lead to $Z_{\rm eff}$=1.3. No plasma currents and drifts are included. The geometry is assumed to be up-down symmetric and only the lower half-domain is modeled; the power from the core into the lower half-domain, $P_{1/2}$ is used as a control parameter.

III. SIMULATION RESULTS

As the input power $P_{1/2}$ is lowered, keeping all other parameters fixed, the simulated divertor enters the detached state. This is illustrated for the XPTD configuration in Figs. (3,4,5).

Low plasma temperature and density near the target plates, and high neutral gas density there, all indicate that for $P_{1/2}$=3 MW, the divertor plasma is detached. The radiation zone is localized near the secondary X-point. As Fig. (5) shows, at lower $P_{1/2}$ the radiation front location shifts closer to the main X-point. Eventually, as the input power $P_{1/2}$ is reduced even lower the radiation front location shifts all way to the main X-point. As this is strongly reminiscent of the MARFE phenomenon, in these simulations this is taken as the onset of a MARFE, which sets the lower bound on the allowable input power for detached operation. Remarkably, there is quite a large window in $P_{1/2}$ when plasma is fully detached; but the detachment front is a safe distance away from the main X-point.

Qualitatively similar behavior is found scanning the input power parameter $P_{1/2}$ for the SXD and LVLD divertor configurations, as is illustrated in Figs. (6,7,8) and in Figs. (9,10,11), respectively.

For the standard divertor, SVPD, detached plasma might exist, but only at low input power, and the radiation front would be close to the main X-point; so by our definition there is little, if any, range of $P_{1/2}$ for detached operation.

These results can be conveniently shown all together for the four studied configurations in a diagram in Fig. (12) where the maximum temperature on the outer plate is plotted vs. $P_{1/2}$. Plasma temperature near the plate below 5 eV is usually a good indication of detachment, and the value of $P_{1/2}$ when plasma temperature on the plate drops below 5 eV (green zone in the Figure) is taken as the threshold of entering detachment. On the other hand, the onset of a MARFE is taken to be the value of $P_{1/2}$ when the radiation zone touches the primary X-point (red zone in the Figure).

It is interesting to note that a typical Alcator C-Mod operating state (about 1 MW of power entering the SOL and about 10 eV temperature on the target plates) is right on the SVPD curve. This is not an accident; after all, the parameters of ADX are close to parameters of C-Mod, and with a standard divertor the regime is close to that of C-Mod, as expected.

In Fig. (12) one can observe that a large parameter window with a detached divertor exists for all three long-legged configurations, while for the standard divertor (SVPD) detached plasma might exist only for very low input power. Radially or vertically extended outer legs appear beneficial for detached operation, and a long vertical leg (LVLD) allows entering detachment at about the

same power as a radially extended leg (SXD). Furthermore, the secondary X-point in the outer leg (XPTD) significantly extends the detached operation window.

IV. ANALYSIS OF SIMULATIONS

The simulations results shown above require detailed analysis to develop physics insight and understand the interplay of the model equations' physics terms in numerical solutions with a detached divertor. Specifically, some questions to address are: What are the radial and poloidal fluxes of plasma and neutral density, momentum, and energy flux? What sets the position of the detachment front? How sensitive are these solutions to model details such as handling impurity ions and neutrals? What are the limits of the power handling capability? Can this regime be scaled to reactor parameters? Here we present an initial attempt to address these questions.

Given the semi-quantitative similarity of the detachment results for all three long-legged divertor configurations, a single representative case is chosen for detailed analysis; a fully detached case in SXD configuration with $P_{1/2}$=0.6 MW, with plasma profiles shown in Fig. (13).

First, consider particle fluxes for each of the radial and poloidal surfaces bounding the leg domain, as shown in Fig. (14). Both the plasma recycling coefficient and neutral albedo are unity so there is no loss of particles at any of the material surfaces; therefore plasma and neutral fluxes through each of the domain boundaries are exactly opposite. From Fig. (14) one can conclude that poloidal fluxes entering/leaving the leg domain are tiny compared to radial fluxes.

Thus the poloidal plasma flow in the divertor leg is weak, according to the particle balance analysis; and to understand this one needs to analyze the parallel plasma momentum balance. This can be conveniently done using the plasma pressure conservation relation that is derived from the standard plasma parallel momentum equation and integrating it along a magnetic field line neglecting some small terms. The resulting pressure conservation relation is similar in form to the Bernoulli law:

$$p_{ei} + m_i n_i \frac{u_{i||} u_{i\theta}}{\sin(\alpha)} + R_\psi + R_\eta + R_{in} = \text{const}, \tag{1}$$

where α is the magnetic line pitch angle, and R_ψ, R_η, R_{in} are terms representing the effects of radial convection, plasma viscosity, and ion-neutral friction[15].

Comparison to Eq. (1) is illustrated in Fig. (15) where different combinations of the total pressure components on the separatrix are plotted vs. the poloidal index. One can observe in the Figure that

in the radiation zone (between reference locations A and B) it is mainly the ion-neutral friction force, with some contributions from plasma viscosity and radial convection, that balances the poloidal plasma pressure drop; below the radiation zone (reference location B) the poloidal plasma pressure drop in the leg is almost entirely balanced by interaction with neutrals. More detailed analysis shows that it is specifically charge-exchange that dominates the ion-neutral friction. It is important to note that plasma recombination plays virtually no role in these numerical solutions.

Looking at the radial and poloidal fluxes of energy entering or exiting the outer leg domain, one can notice that about 30% of $P_{1/2}$ enters the outer leg; the rest goes to the outer walls above the primary X-point, and into the inner leg. As Fig. (16) shows, about 50% of the power entering the outer leg goes with plasma and neutral energy flux to its outer wall boundary. A significant component of the energy flux to the material walls is the binding energy of electron-ion pairs recombining on the surface. The rest of the power entering the outer leg is lost with impurity and hydrogen radiation and is approximately evenly deposited on the inner and outer walls of the divertor channel.

The original code runs were done with unity recycling and albedo coefficients. To investigate the effects of imperfect confinement of neutrals, in the representative case the neutral albedo coefficient was slightly relaxed from 1.0 to 0.995, which is equivalent to letting some neutral particles escape from the divertor leg into the main plasma. The result of this, as shown in Fig. (17), is the detachment front shifting toward the target plate. Reducing the neutral albedo a little bit more would result in losing plasma detachment. Similar results are found if the plasma recycling coefficient is slightly reduced. Thus, the overall conclusion is that confinement of neutral particles is a strong knob controlling the position of the detachment front in the studied regime.

V. DISCUSSION

The basic concept of achieving divertor plasma detachment from material walls by a layer of neutral gas was proposed in the mid-1970s[16], and the detached divertor regime was closely looked at in the early stages of ITER design[17]. Since then, however, the ensuing body of extensive experimental work on many tokamaks has shown that the stable location for the radiation front is near the primary X-point, and this was confirmed by a range of analytical and computational modeling studies; see Ref. [18] and references therein.

However, a radiation front located near the main X-point (i.e., close to the H-mode pedestal) has a strong negative effect on the main plasma performance, according to experience in current experiments, which often show that complete detachment leads to a MARFE and usually to a subsequent plasma disruption in L-mode, or to a transition to L-mode for H-mode plasmas[19–25].

As a result, the fully detached regime is currently considered a risky option for tokamak operation; instead, a partially detached divertor regime is sought, which means that plasma in some flux tubes is detached from the divertor plate but elsewhere it is not. For example the current plans for ITER operation assume a partially detached divertor[11].

Although numerical solutions with fully detached divertors have been documented in the literature, such solutions are usually fragile, requiring careful choice of model parameters, and with a small change of parameters easily transitioning to either a MARFE-like state or an attached state. For example the fully-detached state in UEDGE simulations in Ref. [26] transitions to a MARFE-like state as the input power is reduced by ∼50%. The fully detached state in another study with UEDGE[27] transitions to the attached state with a relatively small tilting of the target plate. Simulations with EDGE2D-EIRENE and SOLPS for upstream density ramp in JET in Ref. [28] show that increasing the upstream density by some 10% beyond detachment onset results in divertor plasma collapse associated with a massive penetration of neutrals to the core, which would likely lead to a disruption in the experiment. SOLPS modeling in Ref. [29] shows that the full detachment regime is correlated with strongly localized radiation in the proximity of the X-point and is prone to a radiation collapse of the plasma in the simulations.

Contrary to the large body of modeling work described in the literature[26–29], the results presented here provide an example of the detached divertor state that persists for a rather broad range of parameters, as was intended in the original gas-box divertor concepts.

Good confinement of neutral gas in the divertor channel is found to be key for maintaining the fully-detached regime in the long-legged configurations studied. This is consistent with results in edge plasma literature. For example, in the AUG divertor experiment and modeling it was found that tilting the target plate inwards is beneficial for detachment while tilting outwards has the opposite effect, because with outward tilt the neutrals can escape the hot plasma region more easily while with inward tilt they are more reflected towards the hot plasma[30]. In recent SOLPS modeling of ITER it was concluded that neutral particle recirculation is key to control of divertor operation[31].

VI. CONCLUSIONS

Several divertor configurations are studied computationally (long or short outer divertor legs, with or without secondary X-points), using the UEDGE code, for parameters matching the design of the ADX tokamak. Steady-state fully detached divertor regimes are found for long-legged tightly baffled divertors for a broad range of parameters. These divertor configurations allow entering a detached state at high input power while keeping the detachment front far away from the main plasma. Furthermore, a secondary X-point in the divertor leg extends the input power window for detached operation by a factor of $\sim$10 compared to a standard divertor. In the studied regimes, neutral particle confinement in the divertor has a very strong effect on the detachment front position. Overall, the presented simulations' results suggest the possibility of robust fully detached operation for a high-power tokamak.

VII. ACKNOWLEDGMENTS

Work performed for U.S. DOE by LLNL under Contract DE-AC52-07NA27344.

REFERENCES

[1]T. Eich, A. Leonard, R. Pitts, W. Fundamenski, R. Goldston, T. Gray, A. Herrmann, A. Kirk, A. Kallenbach, O. Kardaun, A. Kukushkin, B. LaBombard, R. Maingi, M. Makowski, A. Scarabosio, B. Sieglin, J. Terry, A. Thornton, ASDEX Upgrade Team, and JET EFDA Contributors, "Scaling of the tokamak near the scrape-off layer h-mode power width and implications for iter," Nuclear Fusion **53**, 093031 (2013).

[2]P. Valanju, M. Kotschenreuther, S. Mahajan, and J. Canik, "Super-X divertors and high power density fusion devices," Phys. Plas. **70**, 056110 (2009).

[3]H. Takase, "Guidance of divertor channel by cusp-like magnetic field for tokamak devices," J. Phys. Soc. Japan **70**, 609 (2001).

[4]M. Kotschenreuther, "Scrape off layer physics for burning plasmas and innovative divertor solutions," in *Proc. 20nd IAEA Fusion Energy Conference* (IAEA, Vilamoura, Portugal, 2004) CD-ROM file IC/P6-43.

[5]D. D. Ryutov, "Geometrical properties of a snowflake divertor," Physics of Plasmas **14**, 064502 (2007).

[6]D. D. Ryutov and M. V. Umansky, "Divertor with a third-order null of the poloidal field," Physics of Plasmas **20**, 092509 (2013).

[7]B. LaBombard, "ADX: A high field, high power density, advanced divertor and RF tokamak," Nuclear Fusion **55**, 053020 (2015).

[8]D. D. Ryutov and M. V. Umansky, "Ion drifts in a snowflake divertor," Physics of Plasmas **17**, 014501 (2010).

[9]M. V. Umansky and D. D. Ryutov, "Toroidally symmetric plasma vortex at tokamak divertor null point," Physics of Plasmas **23**, 030701 (2016).

[10]B. Lipschultz, B. LaBombard, E. Marmar, M. Pickrell, J. Terry, R. Watterson, and S. Wolfe, "Marfe: an edge plasma phenomenon," Nuclear Fusion **24**, 977 (1984).

[11]R. A. Pitts, "Status and physics basis of the ITER divertor," Physica Scripta **T138**, 014001 (2009).

[12]B. Lipschultz, F. I. Parra, and I. H. Hutchinson, "Sensitivity of detachment extent to magnetic configuration and external parameters," Nuclear Fusion **56**, 056007 (2016).

[13]T. Rognlien, J. Milovich, M. Rensink, and G. Porter, "A fully implicit, time-dependent 2-D fluid code for modeling tokamak edge plasmas," J. Nuc. Mat. **196**, 347–123 (1992).

[14]R. A. Hulse, "Numerical studies of impurities in fusion plasmas," Nuclear Technology - Fusion **3**, 259 (1983).

[15]M. Umansky, D. Brunner, B. LaBombard, and T. D. Rognlien, "Modeling of local edge plasma perturbations induced by a biased probe," Contributions to Plasma Physics **52**, 417–423 (2012).

[16]F. H. Tenney and G. Lewin, "A fusion power plant," Tech. Rep. MAT 1050 (1974).

[17]P.-H. Rebut, D. Boucher, D. J. Gambier, B. E. Keen, and M. L. Watkins, "The ITER challenge," Fusion Engineering and Design **22**, 7–18 (1993).

[18]G. Matthews, "Plasma detachment from divertor targets and limiters," J. Nucl. Materials **220-222**, 104–116 (1995).

[19]A. Loarte, R. Monk, J. Martn-Sols, D. Campbell, A. Chankin, S. Clement, S. Davies, J. Ehrenberg, S. Erents, H. Guo, P. Harbour, L. Horton, L. Ingesson, H. Jckel, J. Lingertat, C. Lowry, C. Maggi, G. Matthews, K. McCormick, D. O'Brien, R. Reichle, G. Saibene, R. Smith, M. Stamp, D. Stork, and G. Vlases, "Plasma detachment in JET Mark I divertor experiments," Nuclear Fusion **38**, 331 (1998).

[20]M. E. Fenstermacher, J. Boedo, R. C. Isler, A. W. Leonard, G. D. Porter, D. G. Whyte, R. D. Wood, S. L. Allen, N. H. Brooks, R. Colchin, T. E. Evans, D. N. Hill, C. J. Lasnier, R. D. Lehmer, M. A. Mahdavi, R. Maingi, R. A. Moyer, T. W. Petrie, T. D. Rognlien, M. J. Schaffer, R. D. Stambaugh, M. R. Wade, J. G. Watkins, W. P. West, and N. Wolf, "Physics of the detached radiative divertor regime in DIII-D," Plasma Physics and Controlled Fusion **41**, A345 (1999).

[21]R. Pitts, B. Duval, A. Loarte, J.-M. Moret, J. Boedo, D. Coster, I. Furno, J. Horacek, A. Kukushkin, D. Reiter, and J. Rommers, "Divertor geometry effects on detachment in {TCV}," Journal of Nuclear Materials **290293**, 940 – 946 (2001), 14th Int. Conf. on Plasma-Surface Interactions in Controlled Fusion Devices.

[22]B. Lipschultz, B. LaBombard, J. Terry, C. Boswell, and I. Hutchinson, "Divertor physics research on alcator c-mod," Fusion science and technology **51**, 369–389 (2007).

[23]A. Kallenbach, M. Bernert, M. Beurskens, L. Casali, M. Dunne, T. Eich, L. Giannone, A. Herrmann, M. Maraschek, S. Potzel, F. Reimold, V. Rohde, J. Schweinzer, E. Viezzer, M. Wischmeier, and the ASDEX Upgrade Team, "Partial detachment of high power discharges in ASDEX-Upgrade," Nuclear Fusion **55**, 053026 (2015).

[24]N. Asakura, N. Hosogane, K. Itami, A. Sakasai, S. Sakurai, K. Shimizu, M. Shimada, H. Kubo, S. Higashijma, H. Takenaga, H. Tamai, S. Konoshima, T. Sugie, K. Masaki, Y. Koide, O. Naito,

H. Shirai, T. Takizuka, T. Ishijima, S. Suzuki, and A. Kumagai, "Role of divertor geometry on detachment and core plasma performance in {JT60U}," Journal of Nuclear Materials **266269**, 182 – 188 (1999).

[25]F. Reimold, M. Wischmeier, M. Bernert, S. Potzel, A. Kallenbach, H. Mller, B. Sieglin, U. Stroth, and the ASDEX Upgrade Team, "Divertor studies in nitrogen induced completely detached h-modes in full tungsten ASDEX-Upgrade," Nuclear Fusion **55**, 033004 (2015).

[26]R. E. Nygren, D. F. Cowgill, M. A. Ulrickson, B. E. Nelson, P. J. Fogarty, T. Rognlien, M. E. Rensink, A. Hassanein, S. S. Smolentsev, and M. Kotschenreuther, "Design integration of liquid surface divertors," Fusion Engineering and Design **72**, 223 (2004).

[27]M. E. Rensink and T. D. Rognlien, "Plasma heat-flux dispersal for ACT1 divertor," Fusion Science and Technology **67**, 125 (2015).

[28]C. Guillemaut, R. Pitts, A. Kukushkin, J. Gunn, J. Bucalossi, G. Arnoux, P. Belo, S. Brezinsek, M. Brix, G. Corrigan, S. Devaux, J. Flanagan, M. Groth, D. Harting, A. Huber, S. Jachmich, U. Kruezi, M. Lehnen, C. Marchetto, S. Marsen, A. Meigs, O. Meyer, M. Stamp, J. Strachan, S. Wiesen, M. Wischmeier, and J. E. Contributors, "Influence of atomic physics on EDGE2D-EIRENE simulations of JET divertor detachment with carbon and beryllium/tungsten plasma-facing components," Nuclear Fusion **54**, 093012 (2014).

[29]F. Reimold, M. Wischmeier, M. Bernert, S. Potzel, D. Coster, X. Bonnin, D. Reiter, G. Meisl, A. Kallenbach, L. Aho-Mantila, and U. Stroth, "Experimental studies and modeling of complete h-mode divertor detachment in ASDEX-Upgrade," Journal of Nuclear Materials **463**, 128 – 134 (2015), proceedings of the 21st International Conference on Plasma-Surface Interactions in Controlled Fusion Devices Kanazawa, Japan May 26-30, 2014.

[30]R. Schneider, X. Bonnin, K. Borrass, D. P. Coster, H. Kastelewicz, D. Reiter, V. A. Rozhansky, and B. J. Braams, "Plasma edge physics with B2-EIRENE," Contributions to Plasma Physics **46**, 3–191 (2006).

[31]A. S. Kukushkin and H. D. Pacher, "Neutral recirculation - the key to control of divertor operation," in *Proc. 1st IAEA Technical Meeting on Divertor Concepts* (IAEA, Vienna, Austria, 2015).

VIII. FIGURE CAPTIONS

FIG. 1. For same dimensions and parameters of ADX, target plates are placed at different locations to produce a SVPD, a SXD, and XPTD configurations. In addition a configuration with a vertically extended leg is considered. Up-down symmetry is assumed and the computational domain includes only the lower half, below the symmetry plane.

FIG. 2. The projected ADX SOL radial profiles are matched using properly chosen transport coefficients in UEDGE; radially growing density diffusion coefficient $D_\perp$ is needed to match the density profile width $\sim$5 mm. Spatially constant $\chi_{e,i}$ is sufficient to achieve $\sim$3 mm width of mid-plane $T_{\perp,e,i}$.

FIG. 3. XPTD for $P_{1/2}$=3 MW. The outer leg is in full detachment, as can be seen from all plasma parameters near target plates: the temperature is on the order of 1 eV, plasma density is low while the outer leg volume fills up with neutral gas. The peak of plasma impurity radiation is localized near the secondary X-point.

FIG. 4. XPTD for $P_{1/2}$=1.6 MW. As the input power is reduced the radiation zone shifts a little bit upstream, the temperature in the divertor leg drops further, and more neutral gas accumulates in the leg.

FIG. 5. XPTD for $P_{1/2}$=0.6 MW. The detachment front shifts further toward the main X-point. Below the detachment front all volume is filled with neutral gas. Plasma density is very low below the detachment front. Eventually, as the input power is reduced, the detachment front would move all way to the main X-point which we would define as MARFE in our model.

FIG. 6. SXD for $P_{1/2}$=1.2 MW. The detachment front is near the plate.

FIG. 7. SXD for $P_{1/2}$=0.8 MW. As the power is reduced further the detachment front shifts upstream.

FIG. 8. SXD for $P_{1/2}$=0.6 MW. As the power is reduced further the detachment front shifts upstream.

FIG. 9. LVLD for $P_{1/2}$=1.2 MW. The detachment front is near the plate.

FIG. 10. LVLD for $P_{1/2}$=0.8 MW. As the power is reduced further the detachment front shifts upstream.

FIG. 11. LVLD for $P_{1/2}$=0.6 MW. As the power is reduced further the detachment front shifts upstream.

FIG. 12. The peak temperature on the outer plate is plotted vs. the input power. In the case of XPTD it is three outer plates, which are labeled by numbers 2,3,4. In all configurations, there is a threshold power where temperature on the plate drops to essentially zero - that is the detachment transition.

FIG. 13. A representative case: SXD with $P_{1/2}$=0.6 MW. The leg is fully detached, the lower half of it is predominantly filled with neutral particles, plasma density is low.

FIG. 14. Analysis of plasma and neutral density fluxes in divertor for the chosen representative case. SOL flow is stagnant since there is no pumping at material surfaces; poloidal flow can exist only if recycling neutral can exist the leg which is difficult in this long narrow slot arrangement.

FIG. 15. Components of the integrated plasma parallel momentum equation in the leg (integrating from the target plate location) first the thermal pressure (red), then adding to it the ram pressure (orange), then adding to it the ion-neutral interaction term, then the viscosity term, and the radial transport term. In the volume filled with neutral gas the R_{in} term balances plasma pressure, above this boundary it is neutral+viscosity+radial transport.

FIG. 16. Components of energy fluxes through the radial and poloidal boundaries.

FIG. 17. The case with slightly reduced neutral albedo.

Fig. 1

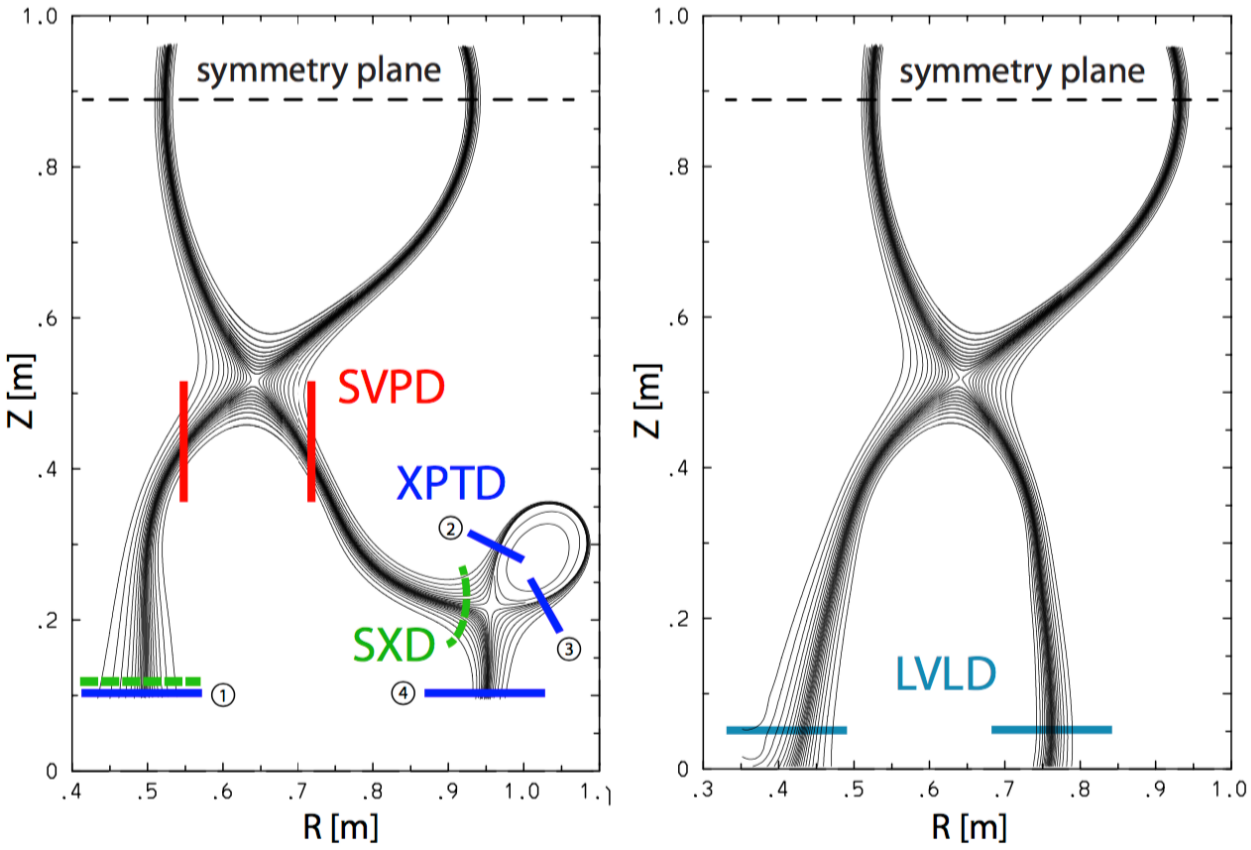
symmetry plane
SVPD
XPTD
SXD
①
②
③
④
Z [m]
R [m]
symmetry plane
LVLD
Z [m]
R [m]

Fig. 2

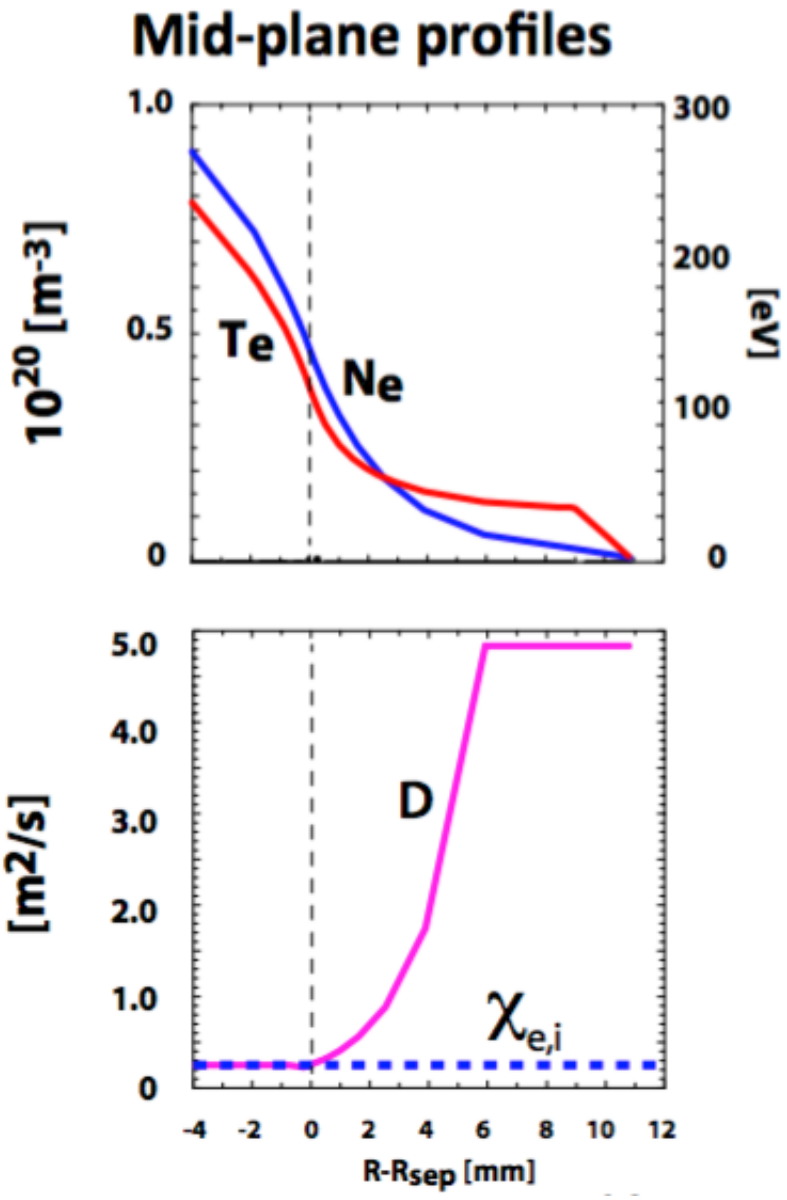
Mid-plane profiles
1.0
0.5
0
300
200
100
0
10^{20} [m^{-3}]
[eV]
Te
Ne
5.0
4.0
3.0
2.0
1.0
0
[m2/s]
D
$\chi_{e,i}$
-4
-2
0
2
4
6
8
10
12
R-R$_{sep}$ [mm]

Fig. 3

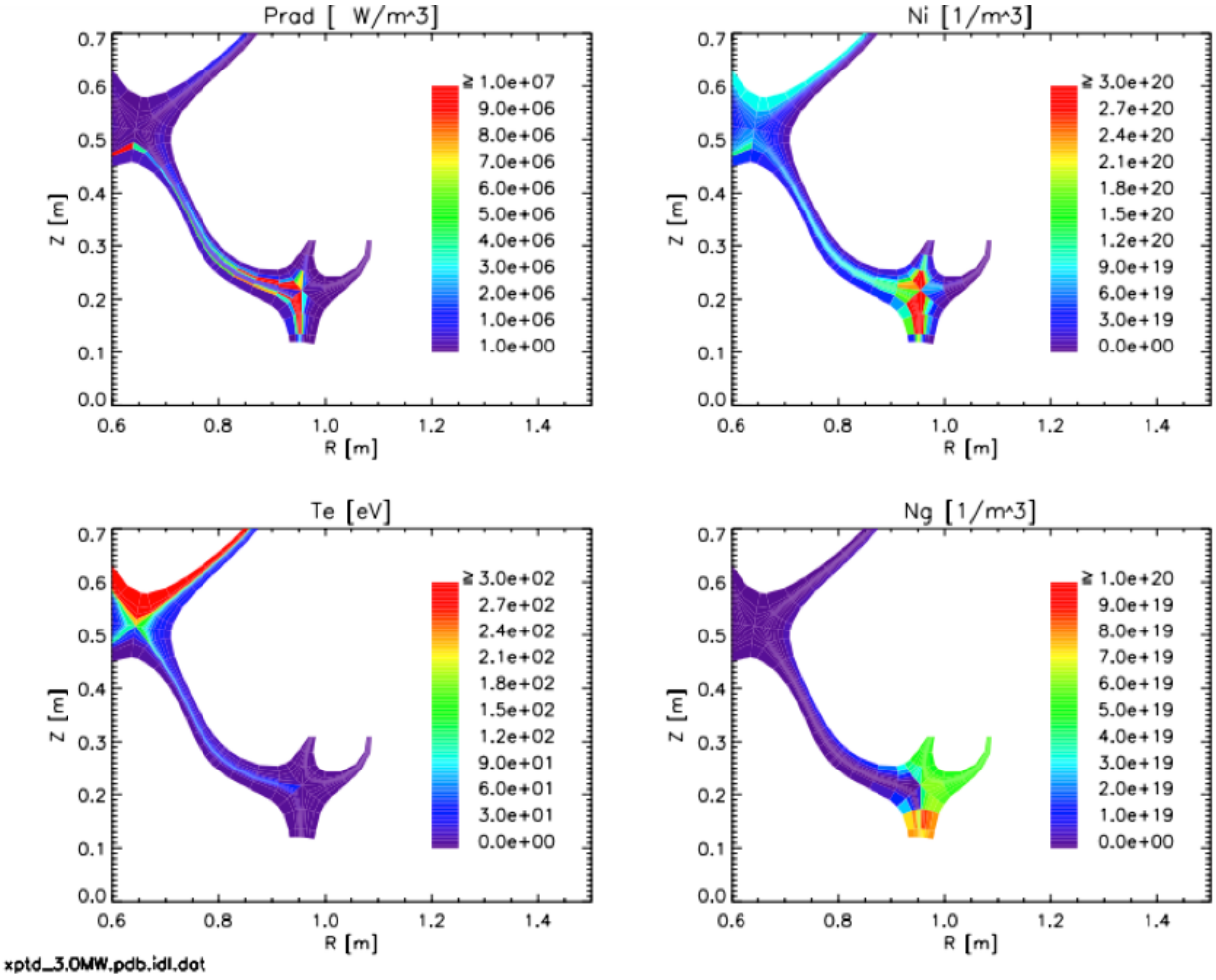
Prad [W/m^3]
≥ 1.0e+07
9.0e+06
8.0e+06
7.0e+06
6.0e+06
5.0e+06
4.0e+06
3.0e+06
2.0e+06
1.0e+06
1.0e+00
Ni [1/m^3]
≥ 3.0e+20
2.7e+20
2.4e+20
2.1e+20
1.8e+20
1.5e+20
1.2e+20
9.0e+19
6.0e+19
3.0e+19
0.0e+00
Te [eV]
≥ 3.0e+02
2.7e+02
2.4e+02
2.1e+02
1.8e+02
1.5e+02
1.2e+02
9.0e+01
6.0e+01
3.0e+01
0.0e+00
Ng [1/m^3]
≥ 1.0e+20
9.0e+19
8.0e+19
7.0e+19
6.0e+19
5.0e+19
4.0e+19
3.0e+19
2.0e+19
1.0e+19
0.0e+00
Z [m]
R [m]
xptd_3.0MW.pdb.idl.dot

Fig. 4

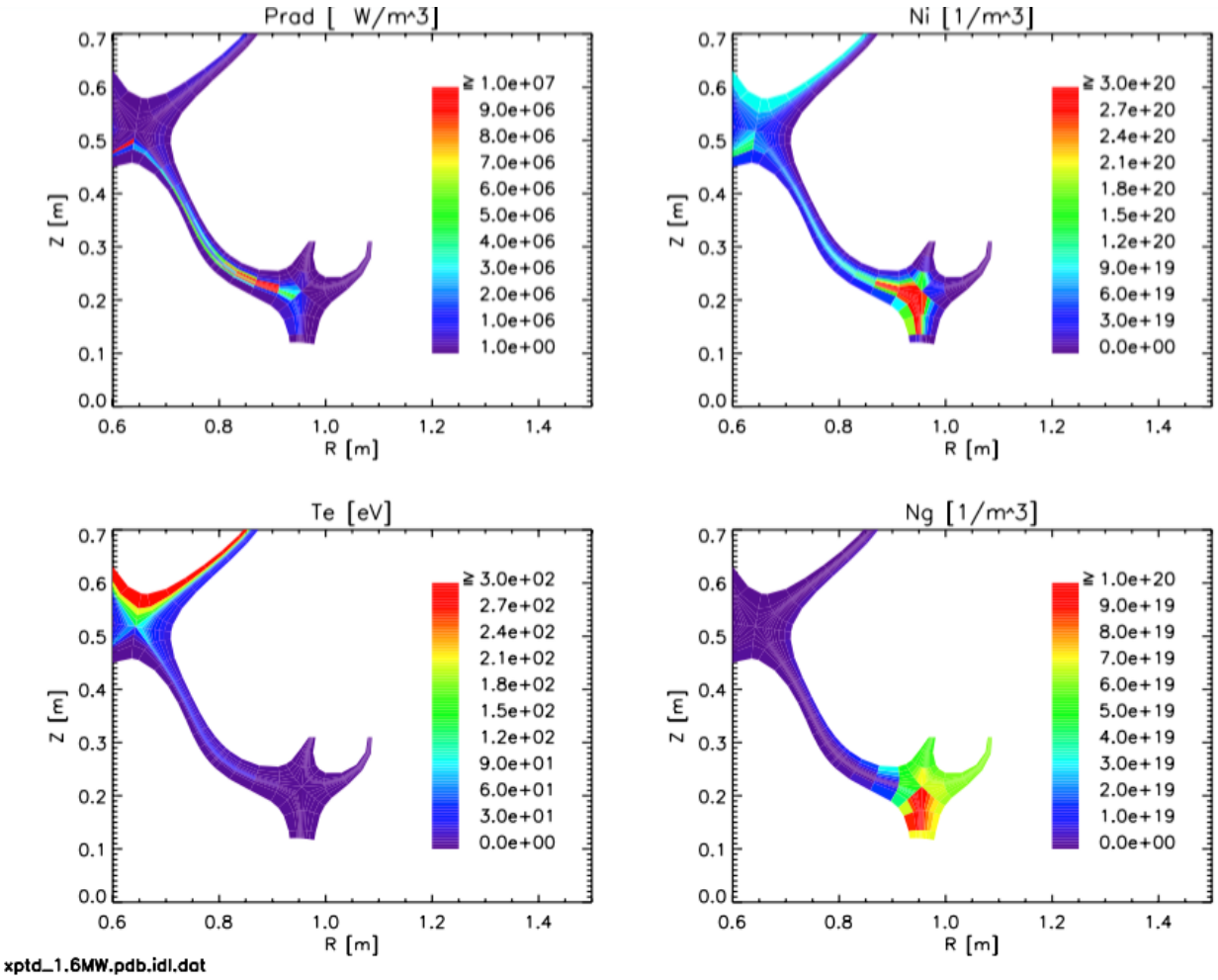

Fig. 5

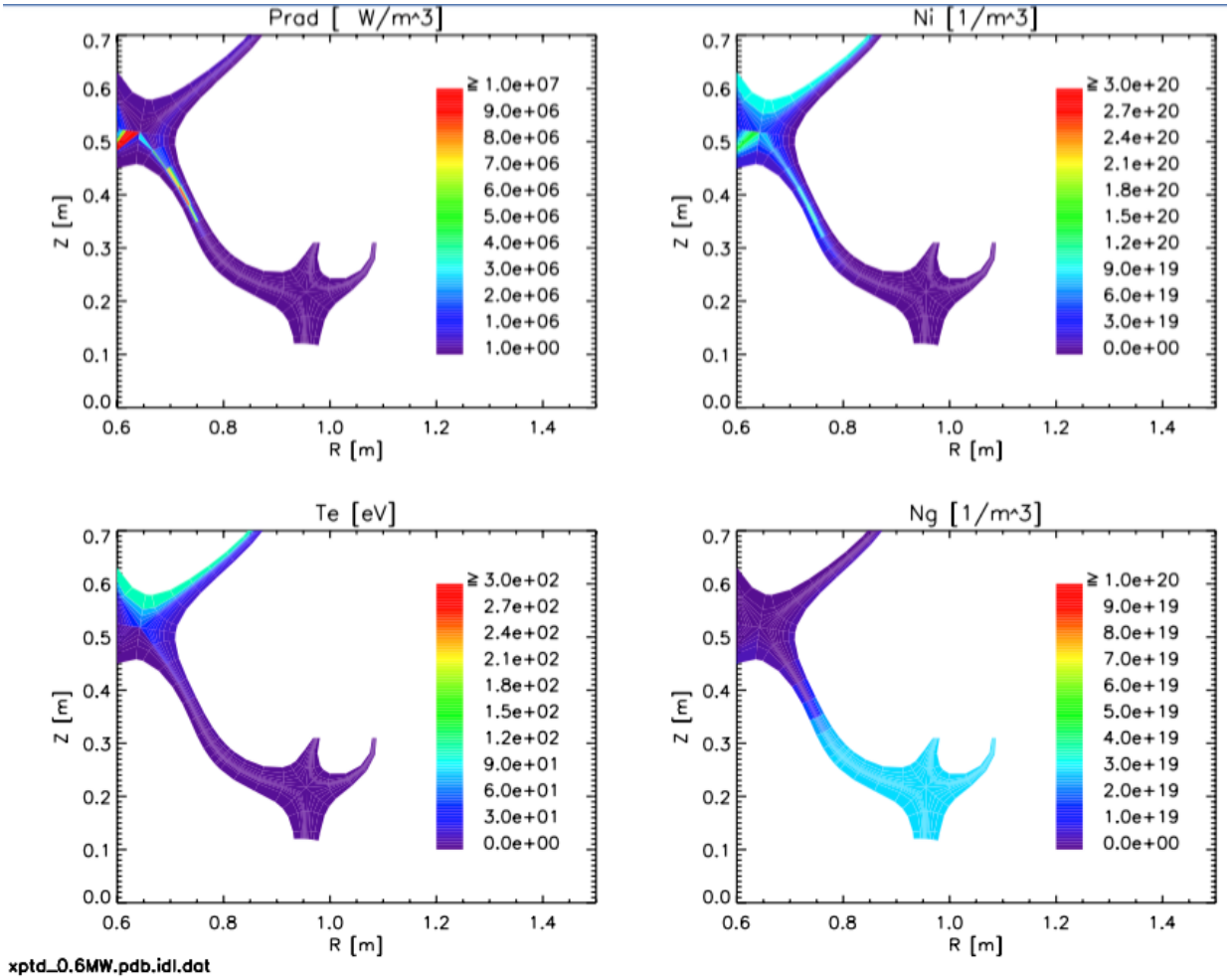

Fig. 6

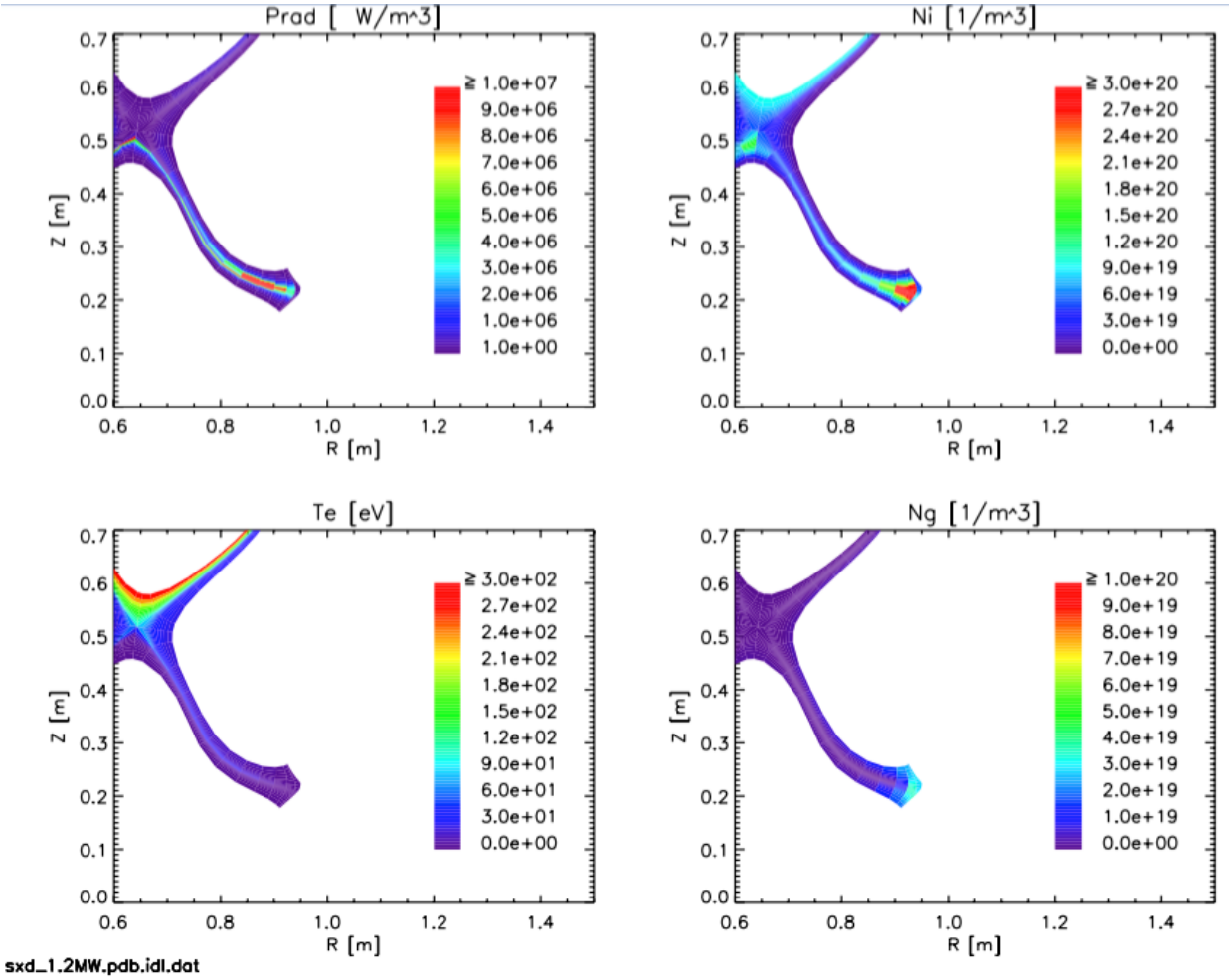
Prad [W/m^3]
1.0e+07
9.0e+06
8.0e+06
7.0e+06
6.0e+06
5.0e+06
4.0e+06
3.0e+06
2.0e+06
1.0e+06
1.0e+00
Ni [1/m^3]
3.0e+20
2.7e+20
2.4e+20
2.1e+20
1.8e+20
1.5e+20
1.2e+20
9.0e+19
6.0e+19
3.0e+19
0.0e+00
Te [eV]
3.0e+02
2.7e+02
2.4e+02
2.1e+02
1.8e+02
1.5e+02
1.2e+02
9.0e+01
6.0e+01
3.0e+01
0.0e+00
Ng [1/m^3]
1.0e+20
9.0e+19
8.0e+19
7.0e+19
6.0e+19
5.0e+19
4.0e+19
3.0e+19
2.0e+19
1.0e+19
0.0e+00
Z [m]
R [m]
sxd_1.2MW.pdb.idl.dat

Fig. 7

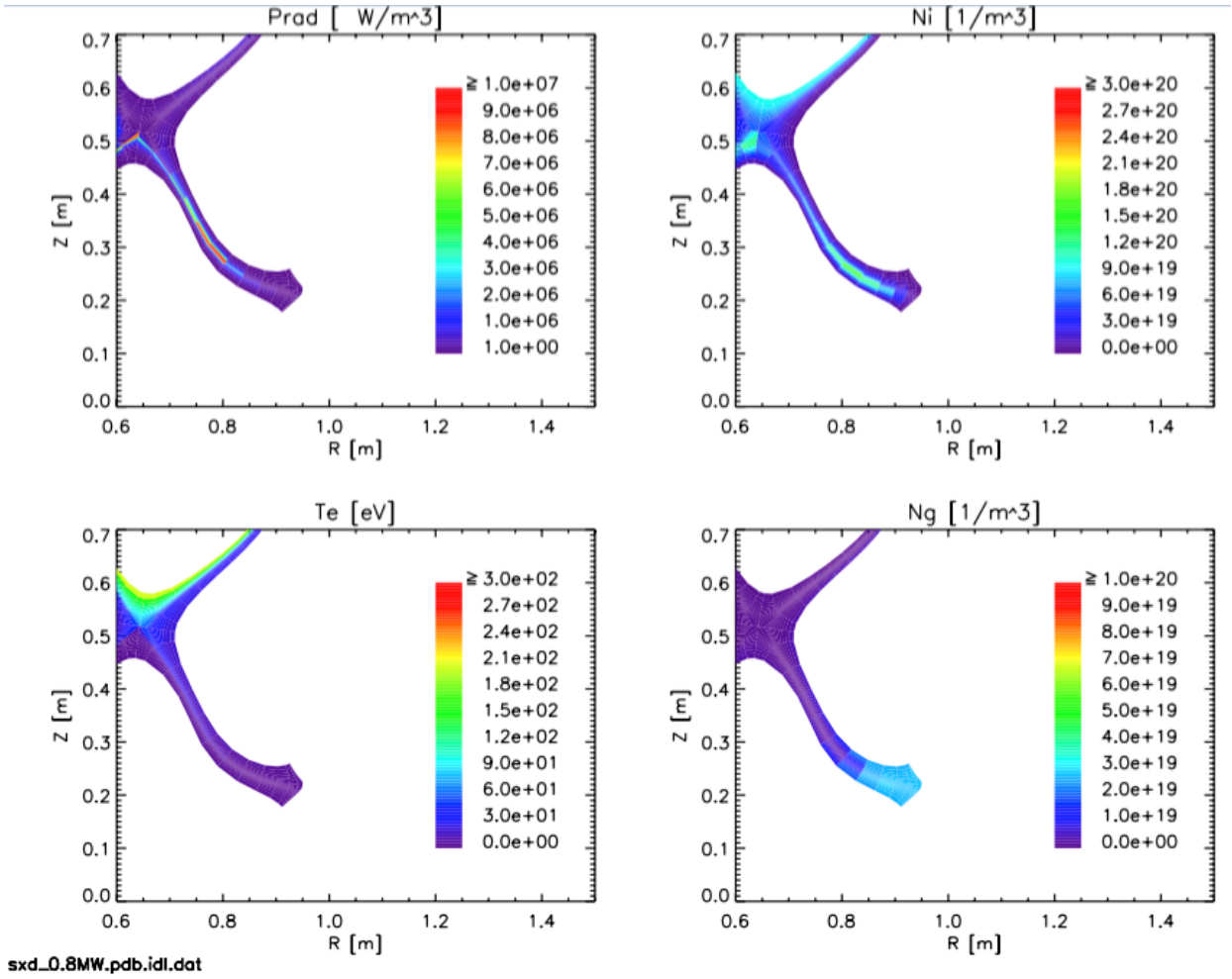

Fig. 8

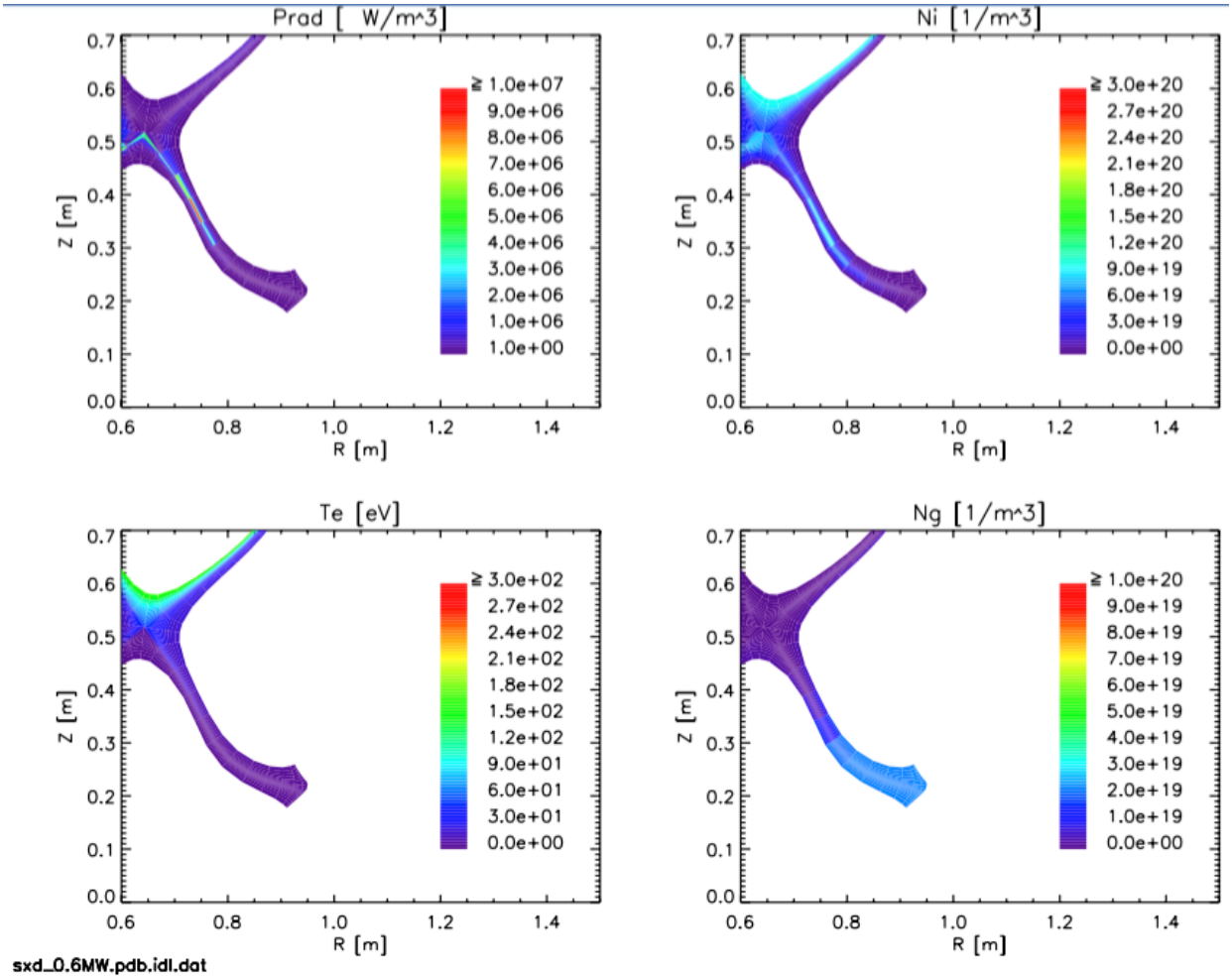

Fig. 9

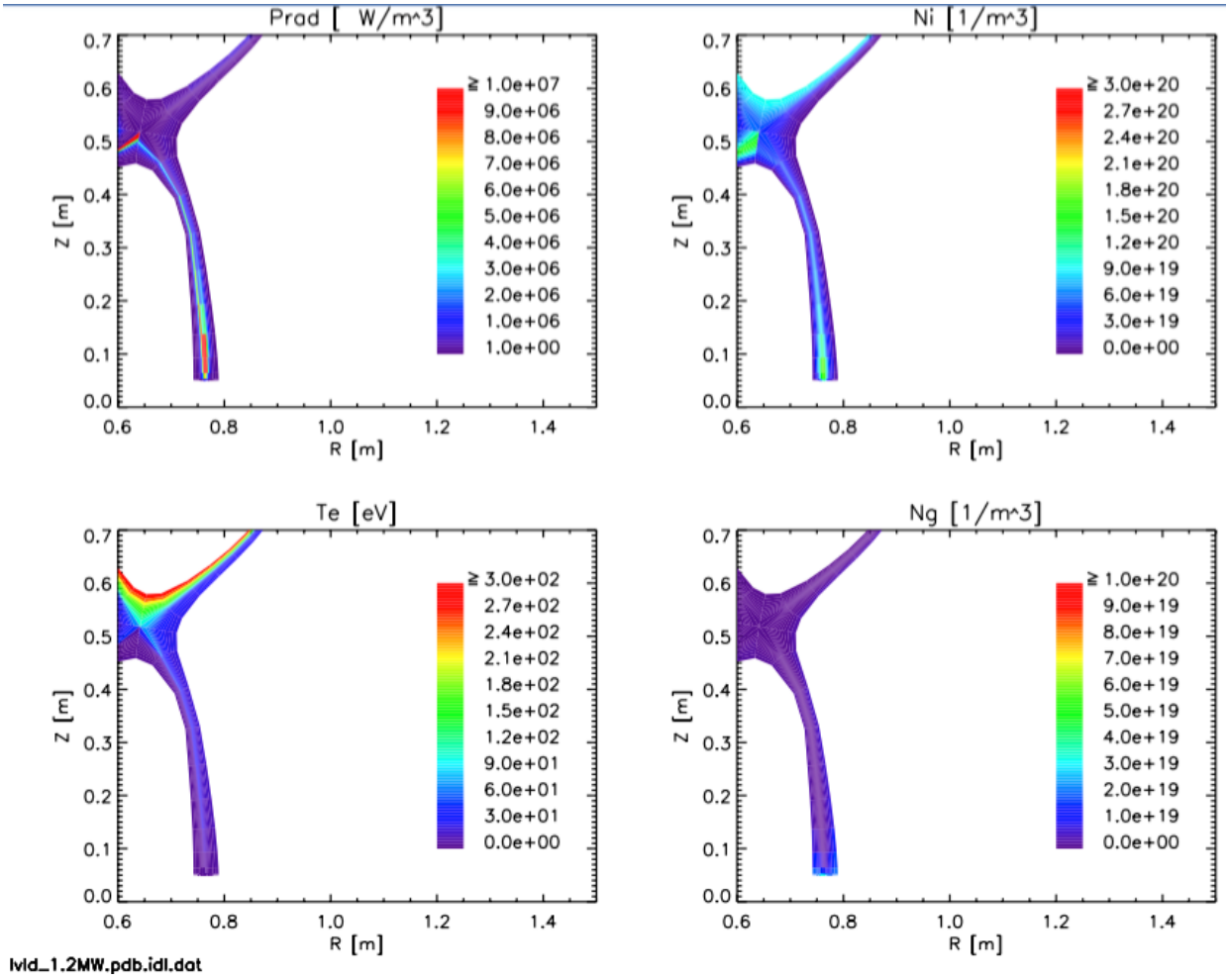
Prad [W/m^3]
1.0e+07
9.0e+06
8.0e+06
7.0e+06
6.0e+06
5.0e+06
4.0e+06
3.0e+06
2.0e+06
1.0e+06
1.0e+00
Ni [1/m^3]
3.0e+20
2.7e+20
2.4e+20
2.1e+20
1.8e+20
1.5e+20
1.2e+20
9.0e+19
6.0e+19
3.0e+19
0.0e+00
Te [eV]
3.0e+02
2.7e+02
2.4e+02
2.1e+02
1.8e+02
1.5e+02
1.2e+02
9.0e+01
6.0e+01
3.0e+01
0.0e+00
Ng [1/m^3]
1.0e+20
9.0e+19
8.0e+19
7.0e+19
6.0e+19
5.0e+19
4.0e+19
3.0e+19
2.0e+19
1.0e+19
0.0e+00
Z [m]
R [m]
Ivid_1.2MW.pdb.idl.dat

Fig. 10

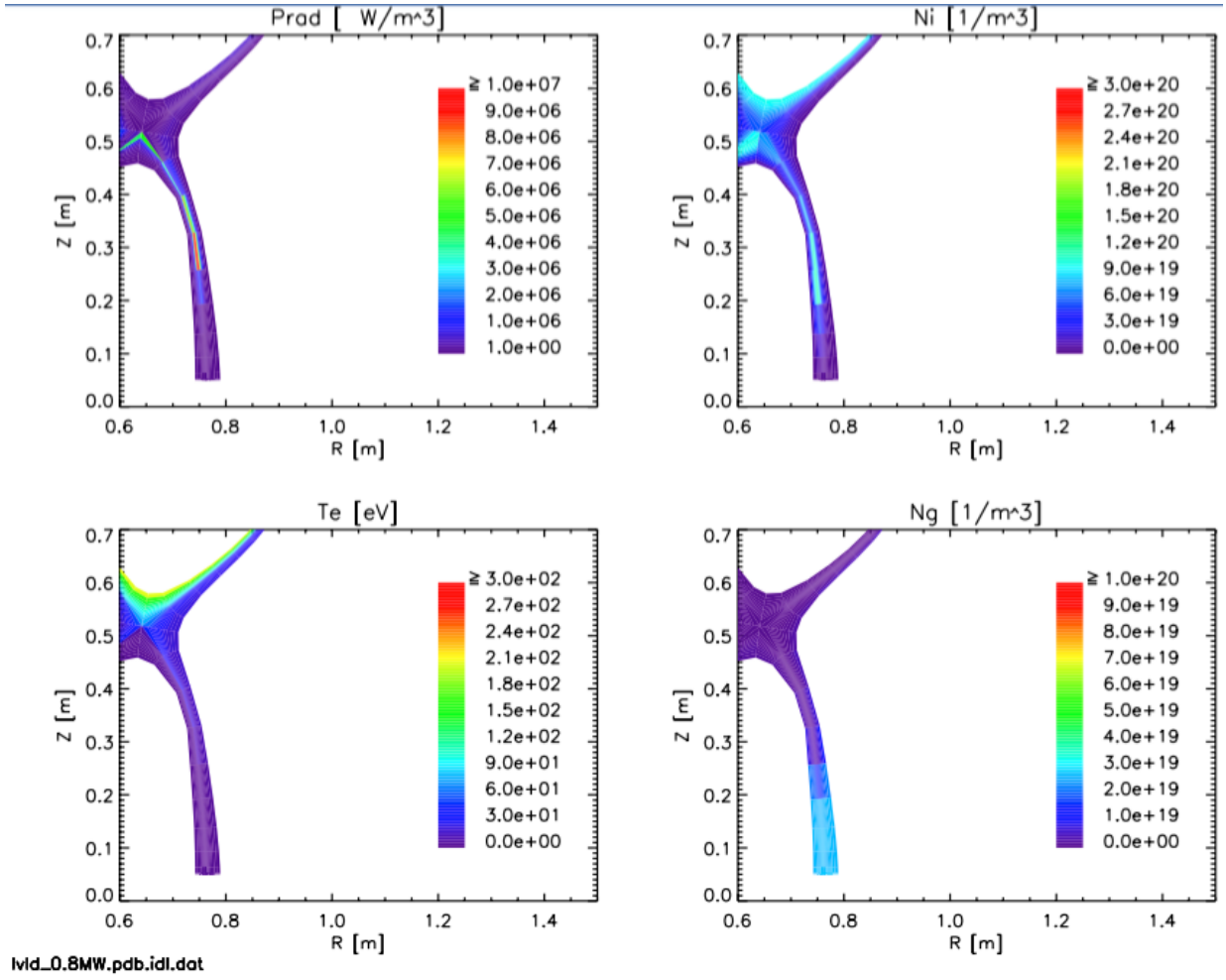

Fig. 11

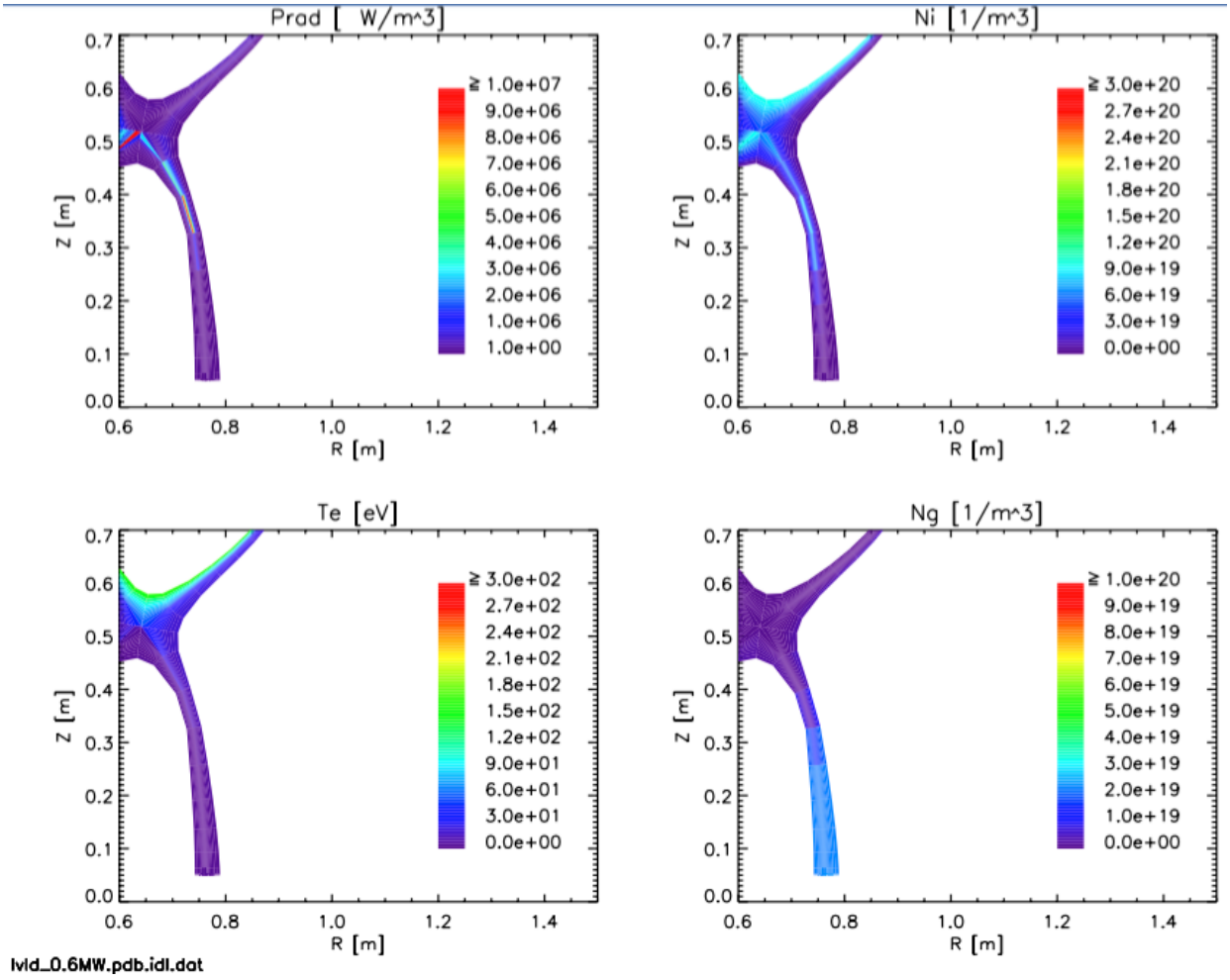

Fig. 12

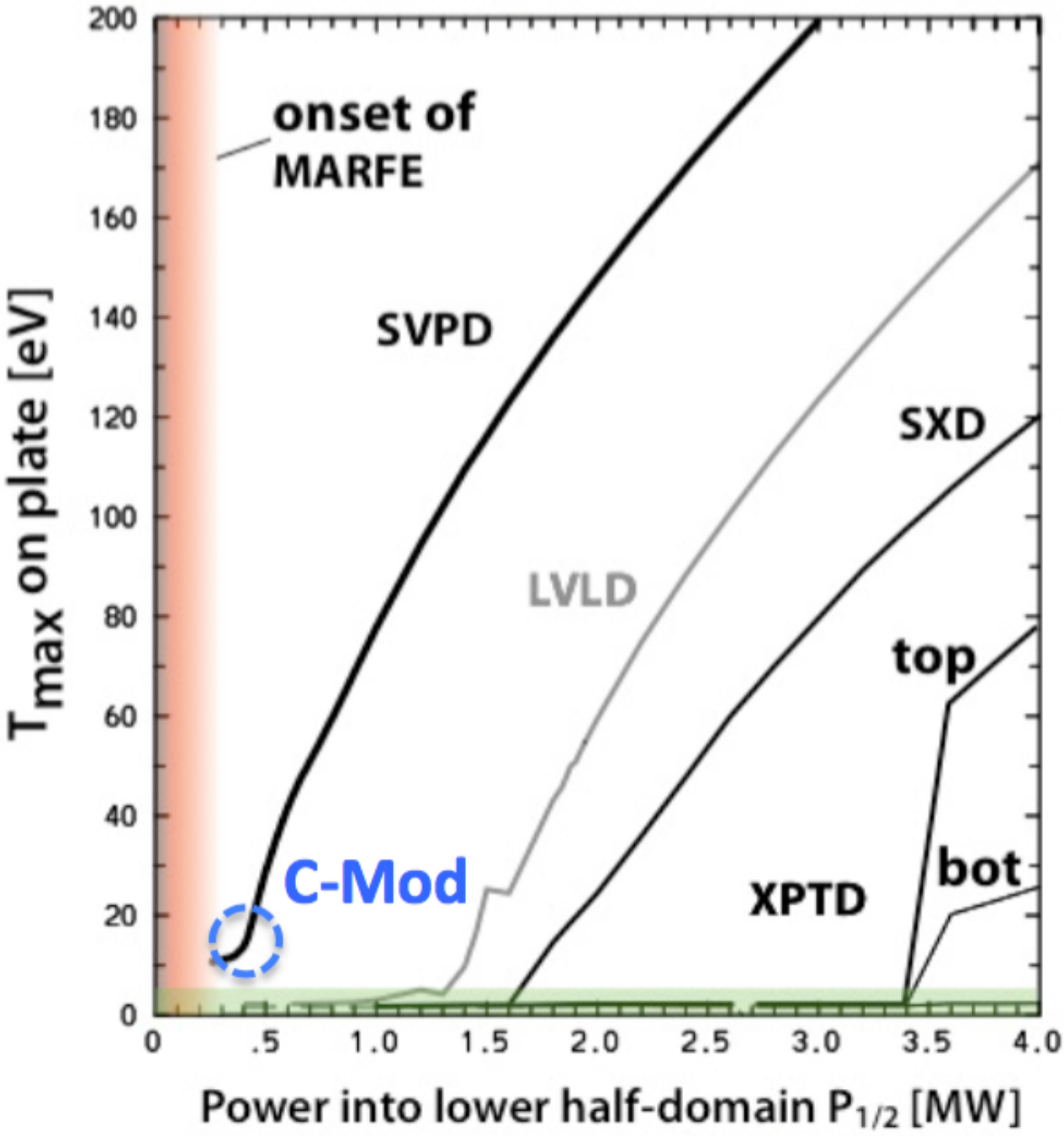
onset of
MARFE
SVPD
SXD
LVLD
top
bot
XPTD
C-Mod
T_{max} on plate [eV]
Power into lower half-domain $P_{1/2}$ [MW]
0
20
40
60
80
100
120
140
160
180
200
0
.5
1.0
1.5
2.0
2.5
3.0
3.5
4.0

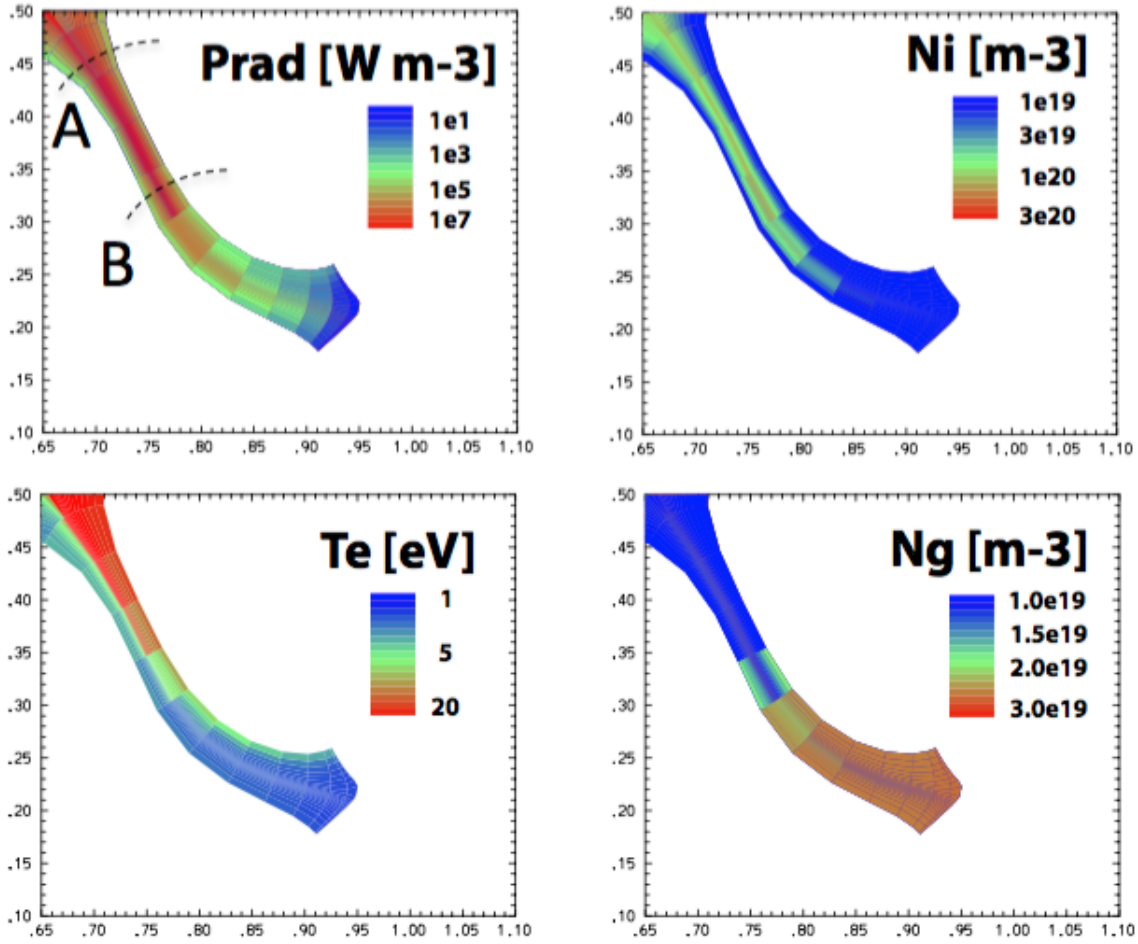
Prad [W m-3]
A
B
1e1
1e3
1e5
1e7
Ni [m-3]
1e19
3e19
1e20
3e20
Te [eV]
1
5
20
Ng [m-3]
1.0e19
1.5e19
2.0e19
3.0e19

Fig. 13

Fig. 14

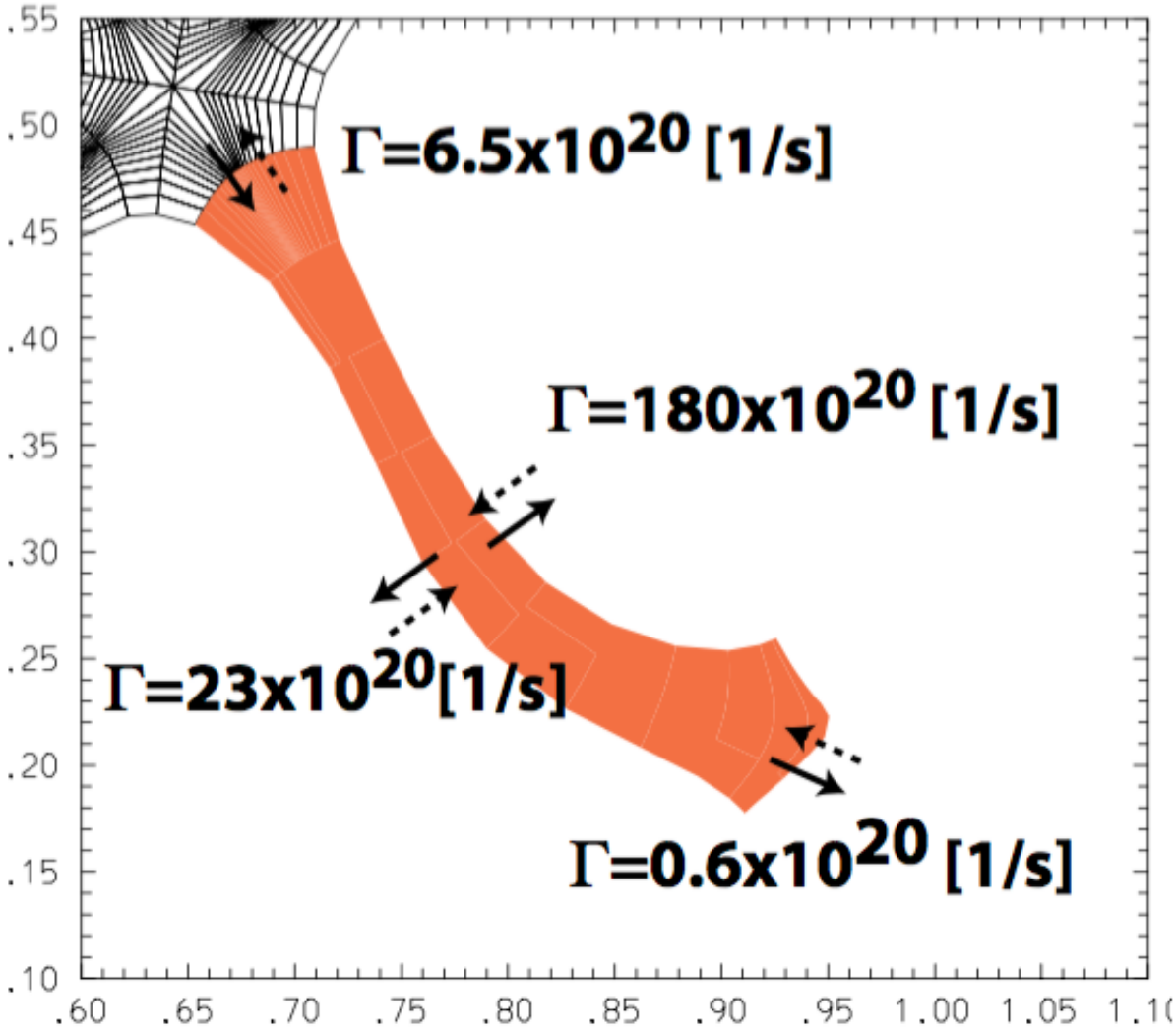
Γ=6.5x10^20 [1/s]
Γ=180x10^20 [1/s]
Γ=23x10^20[1/s]
Γ=0.6x10^20 [1/s]
.55
.50
.45
.40
.35
.30
.25
.20
.15
.10
.60
.65
.70
.75
.80
.85
.90
.95
1.00
1.05

Fig. 15

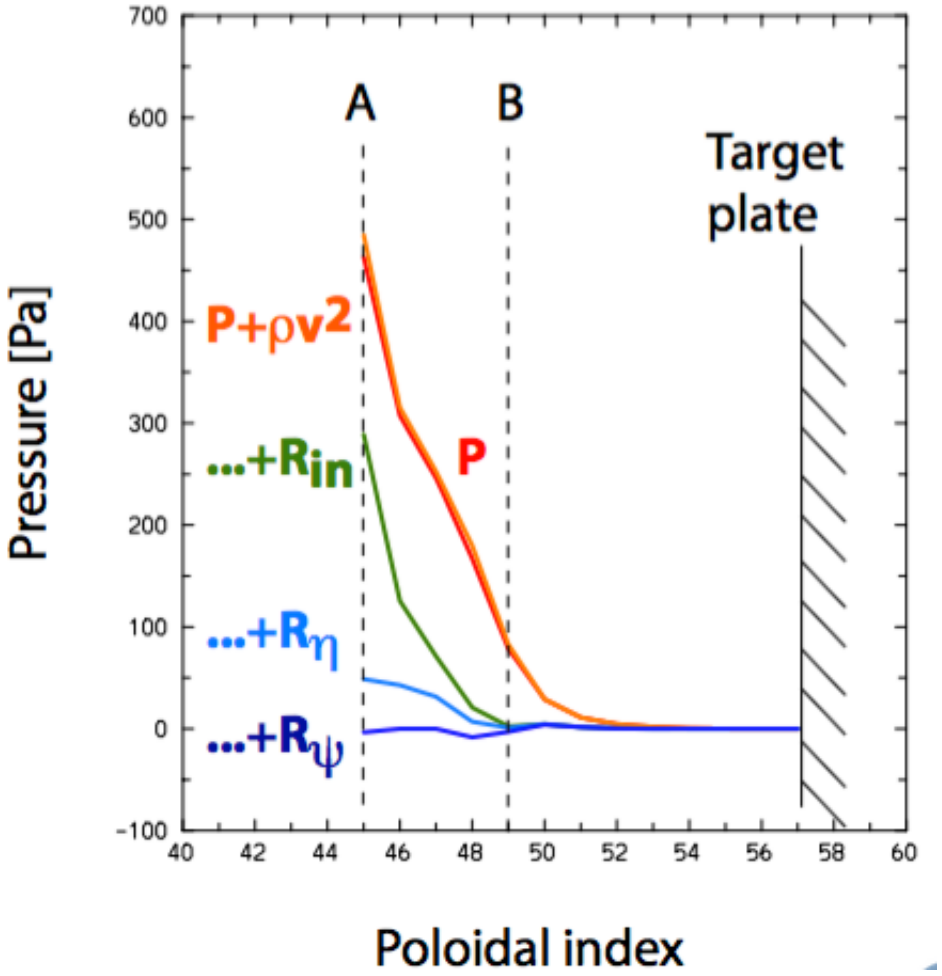
Pressure [Pa]
700
600
500
400
300
200
100
0
-100
40
42
44
46
48
50
52
54
56
58
60
A
B
Target plate
P+ρv2
...+Rin
P
...+Rη
...+Rψ
Poloidal index

Fig. 16

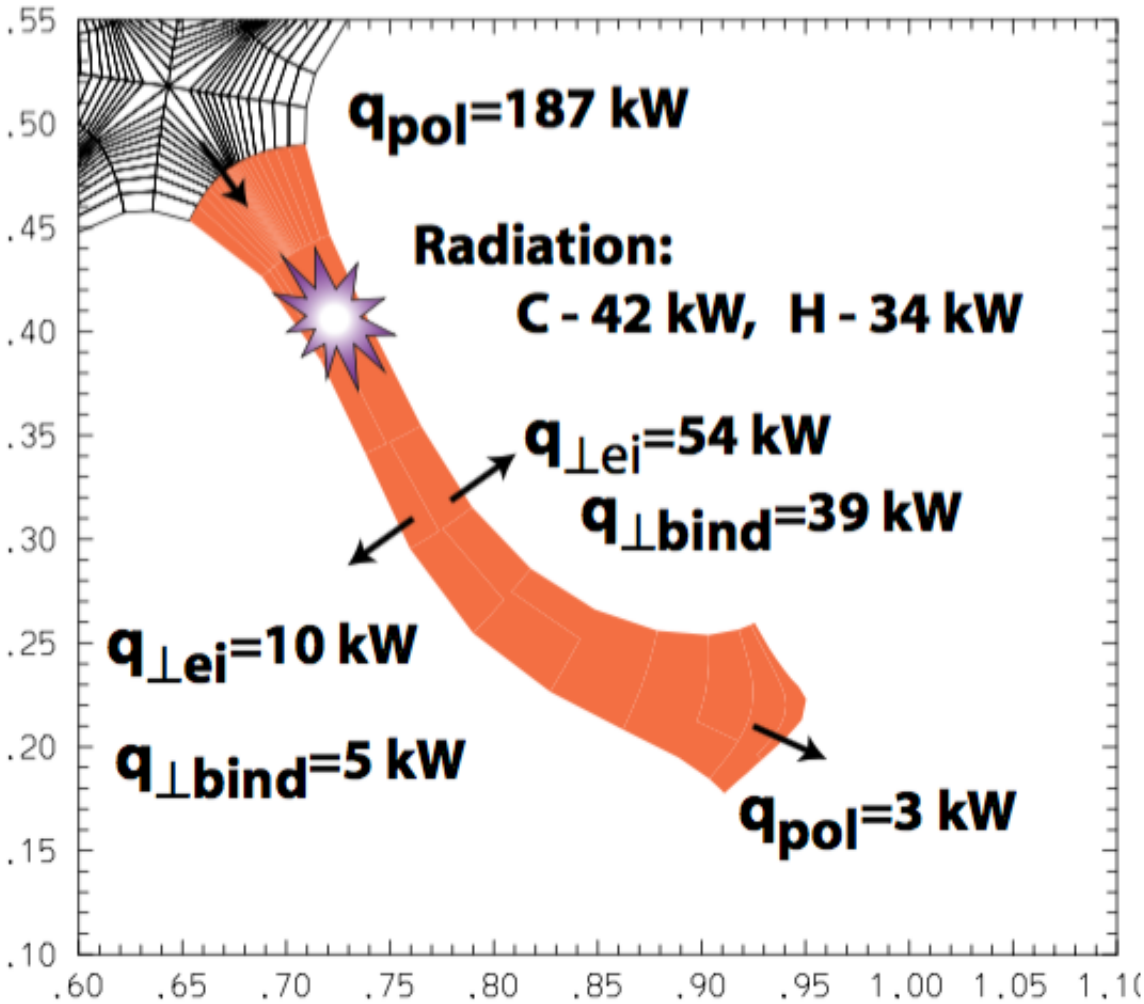
q_{pol}=187 kW
Radiation:
C - 42 kW, H - 34 kW
$q_{\perp ei}$=54 kW
$q_{\perp bind}$=39 kW
$q_{\perp ei}$=10 kW
$q_{\perp bind}$=5 kW
q_{pol}=3 kW
.55
.50
.45
.40
.35
.30
.25
.20
.15
.10
.60
.65
.70
.75
.80
.85
.90
.95
1.00
1.05

Fig. 17

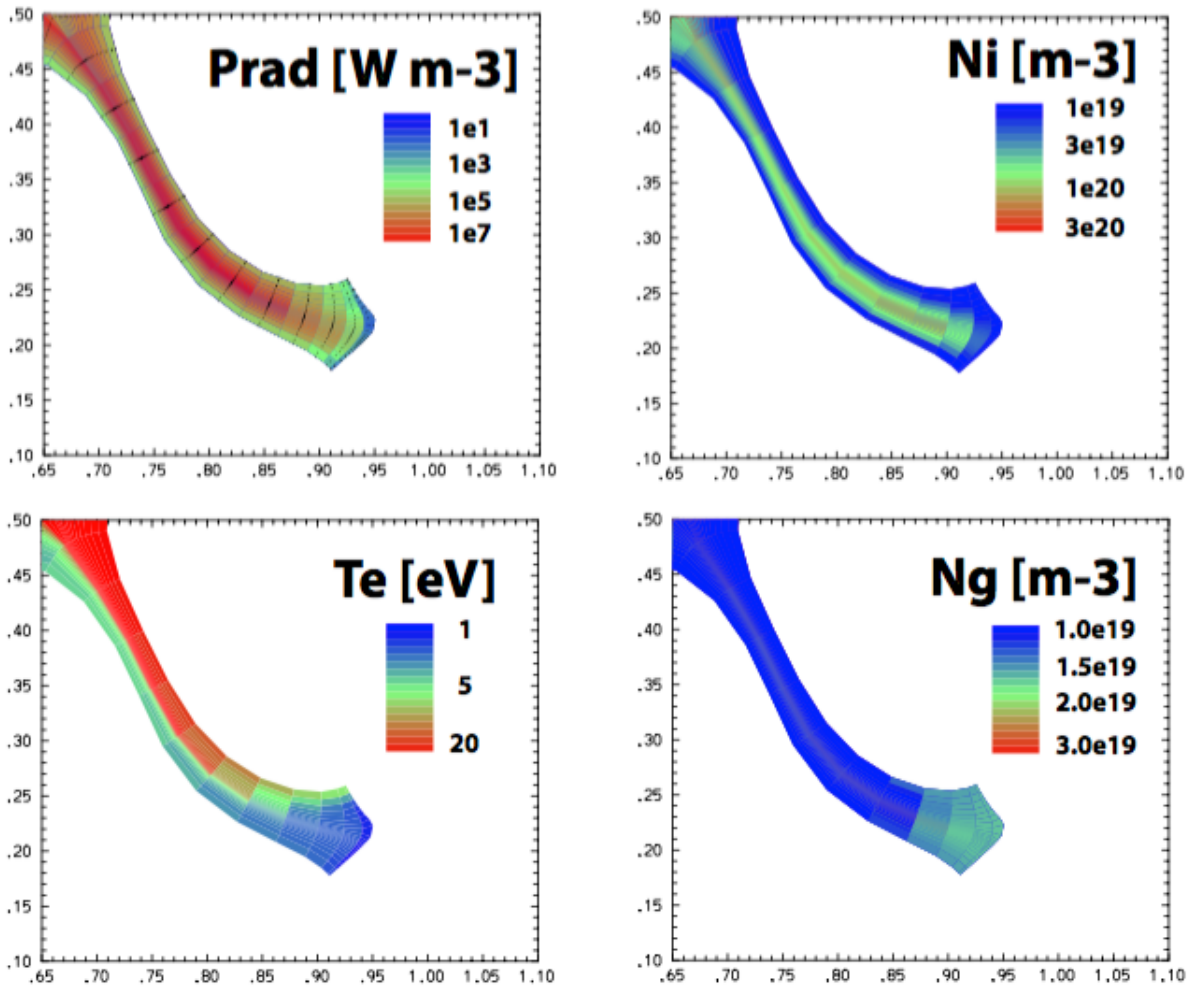
Prad [W m-3]
1e1
1e3
1e5
1e7
Ni [m-3]
1e19
3e19
1e20
3e20
Te [eV]
1
5
20
Ng [m-3]
1.0e19
1.5e19
2.0e19
3.0e19
.50
.45
.40
.35
.30
.25
.20
.15
.10
.65
.70
.75
.80
.85
.90
.95
1.00
1.05
1.10